Supporting Information

The antibiotic novobiocin binds and activates the ATPase that powers lipopolysaccharide transport

Janine M. May,[‡,a] Tristan W. Owens, [‡,a] Michael D. Mandler, [‡,a] Brent W. Simpson,[‡,b] Michael B. Lazarus,[a] David J. Sherman,[a] Rebecca M. Davis,[b] Suguru Okuda,[a,x] Walter Massefski,[c] Natividad Ruiz,*[,b] Daniel Kahne*[,a]

[a]*Department of Chemistry and Chemical Biology, Harvard University, Cambridge, MA 02138, USA*

[b]*Department of Microbiology, The Ohio State University, Columbus, OH 43210, USA*

[c]*Department of Chemistry, Massachusetts Institute of Technology, Cambridge, MA 02139, USA*

Table of Contents

Supplemental Figures and Tables

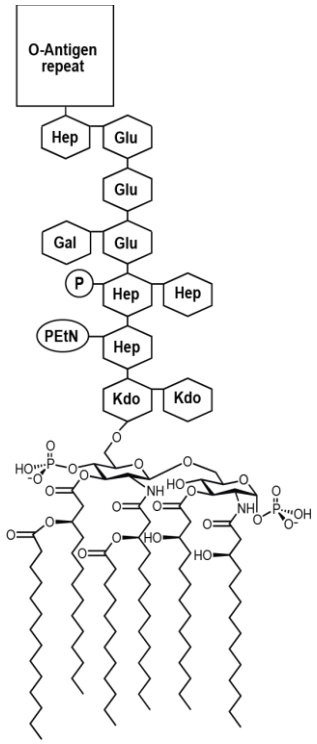

Figure S1. Structure of *E. coli* lipopolysaccharide. Kdo = 3-deoxy-D-manno-oct-2-ulosonic acid, Hep = L-glycero-D-manno-heptose, PEtN = phosphoethanolamine, P = phosphate, Glu = D-glucose, Gal = D-galactose.

	Zone of inhibition (in mm)				
	Bacitracin	**Novobiocin**	**Erythromycin**	**Rifampicin**	**Nalidixic acid**
wild type	<6	<6	(8)	8(9)	11(14)
lptB1	17	14(24)	16(21)	17	18(21)
lptB1(G33C)	(8)	<6	(11)	9	12(14)
lptB1(R144H)	17	<6	(16)	24	17(20)

Table S1. Quantification of antibiotic sensitivity assay in Figure 1b. Lawns of bacteria were grown on LB plates in the presence of disks containing bacitracin, novobiocin, erythromycin, rifampicin, and nalidixic acid. The diameter (in mm) of the zone of total (clear appearance) or partial (hazy appearance; numbers in parenthesis) growth inhibition around the disks was measured as an indicator of antibiotic susceptibility. For an explanation of the effect of erythromycin in *lptB1(R144H)* cells, see Figure S2.

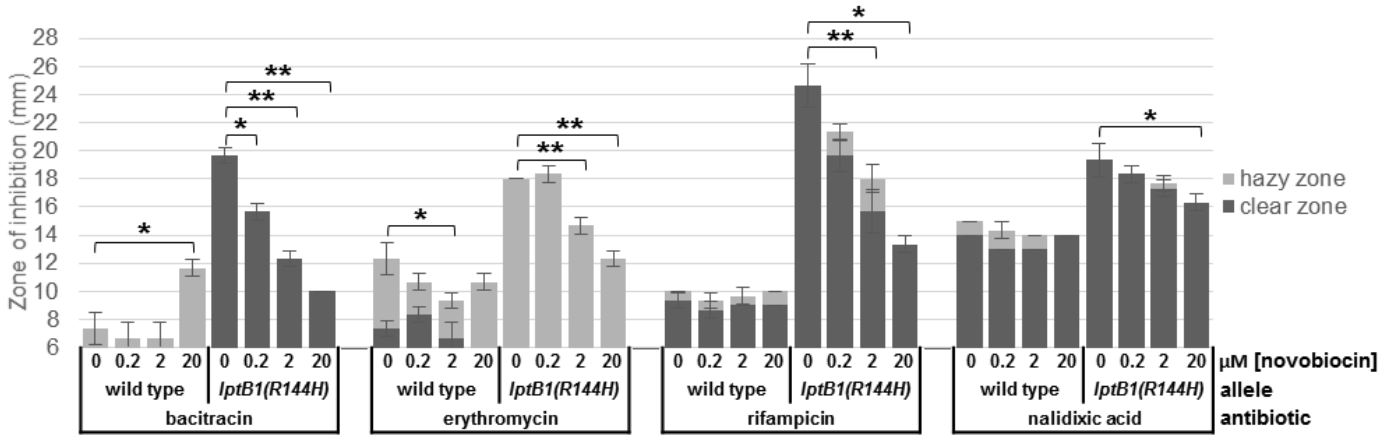

Figure S2. Novobiocin suppresses outer membrane permeability defects of *lptB1(R144H*) in a dose-dependent manner. Disk diffusion assays of wild-type and *lptB1(R144H)* cells on LB agar containing increasing concentrations of novobiocin. The diameter of zones of complete (clear, dark bars) and partial (hazy, light bars) growth inhibition around disks containing bacitracin, erythromycin, rifampicin, and nalidixic acid were measured after overnight growth at 37 °C. Statistical significance demonstrated by paired t-test: $p \leq 0.05$ indicated by * and $p \leq 0.01$ indicated by **. As noted in the main text and Table S1, without novobiocin, the growth around the erythromycin disk is partially restored in *lptB1(R144H)* cells, but to a much less extent than around the novobiocin disk, where total growth is restored. We believe this is due to a different suppression mechanism which we have previously described (1). In Ref (1), our groups described that slowing down growth can suppress LPS transport defects. We hypothesized in that work that by slowing the growth rate of the cell envelope, there was a reduced demand for LPS to be transported to the outer membrane. We see that clear zones of inhibition around erythromycin disks can become hazy in many *lpt* mutants and we think it is likely caused by erythromycin decreasing growth rate as described by Ref (1). The hazy zone of inhibition reflects that slow-growing bacteria. This figure quantitatively shows how an increase in concentration of novobiocin restores *lptB1(R144H)* resistance to hydrophobic antibiotics, including erythromycin, and moreover shows that *lptB1(R144H)* is sensitive to erythromycin.

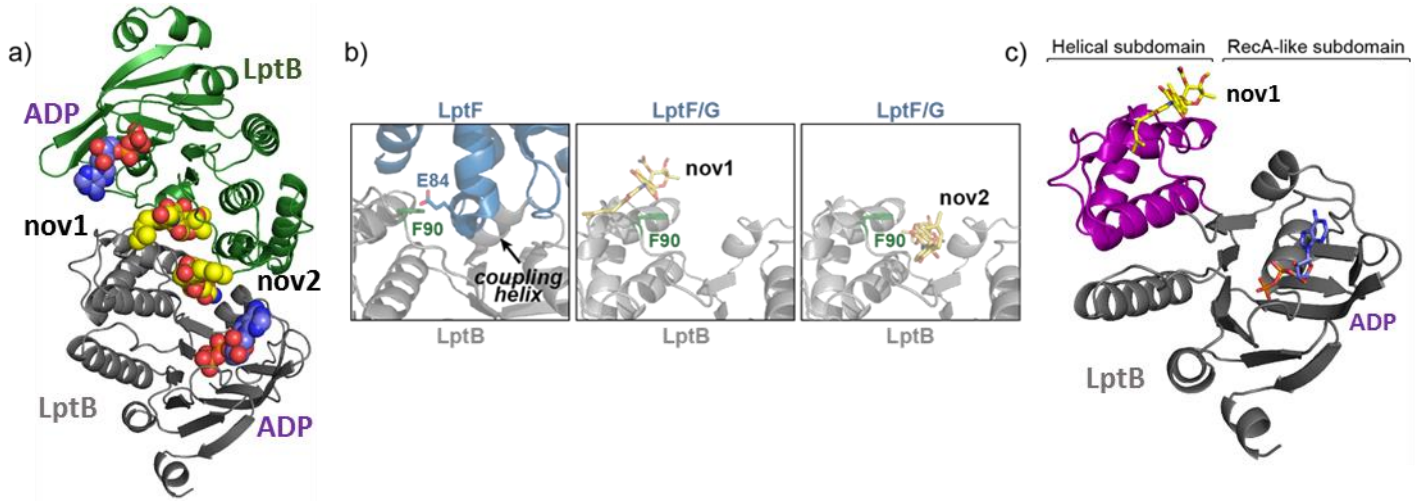

Figure S3. Novobiocin binds at the interface with LptF/G. a) Two molecules of novobiocin were found in the structure (LptB-ADP-NOV) bound symmetrically at the crystallographic dimer interface. b) Comparison of the groove region of LptB and LptF from *Pseudomonas aeruginosa* (PDB: 5X5Y) with that of LptB-ADP-NOV (1). As each LptB monomer contacts both novobiocin molecules, there are two potential novobiocin binding sites (nov1 and nov2). The nov1 site is positioned to the side of the groove, while the nov2 site occludes the groove, suggesting it is not the relevant site. c) The nov1 site is located in the helical subdomain, which coordinates interactions with the transmembrane domains (2).

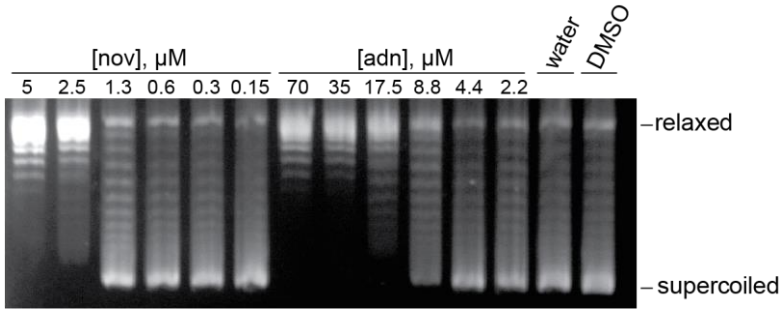

Figure S4. Novobiocin-adamantyl (adn) has reduced activity against DNA gyrase *in vitro* compared to novobiocin (nov). Relaxed DNA was incubated with purified DNA gyrase with and without nov and adn.

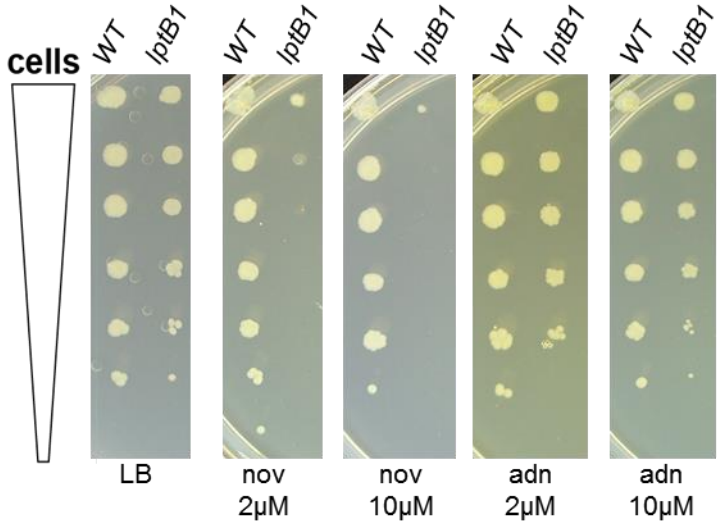

Figure S5. Novobiocin-adamantyl is less potent than novobiocin against *lptB1* cells *in vivo*. Efficiency of plating assay conducted as described in Figure 3B.

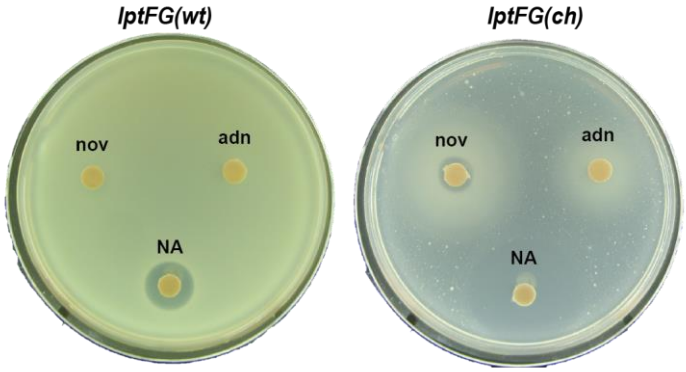

Figure S6. Novobiocin (nov) and novobiocin-adamantyl (adn), but not nalidixic acid (NA), suppress the lethality of *lptFG(ch)*. Strains were grown overnight in minimal media and then plated on LB plates. Each disk contains 5 μg compound.

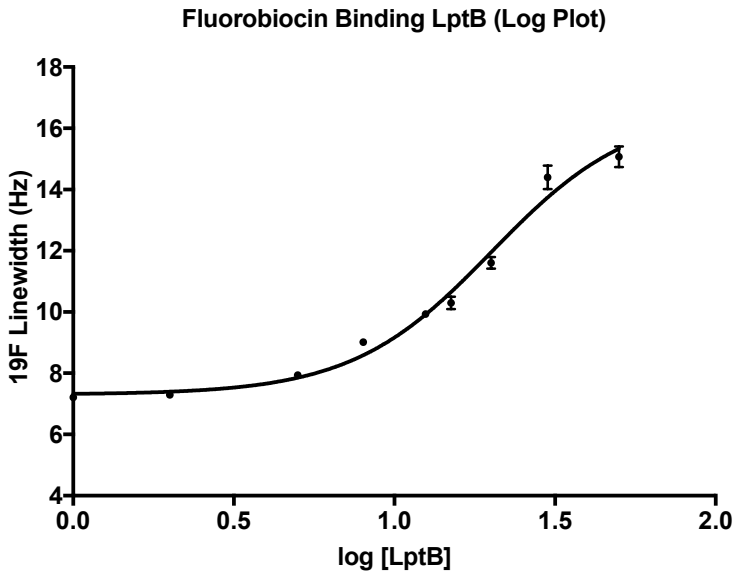

Figure S7. The ^{19}F NMR linewidth of fluorobiocin (**Fbn**) was plotted vs. log[LptB]. Data were analyzed with GraphPad Prism 7 software using a nonlinear fit, log(agonist) vs. response with an $R^2 = 0.98$. Error bars represent the standard error of the mean (±SEM). The K_D was calculated to be 20 ± 9 μM.

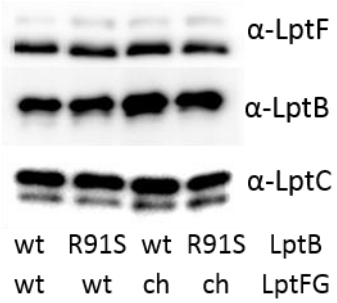

Figure S8. Protein levels are consistent across vesicle preparations. Levels of LptB, LptF, and LptC in vesicles from Figures 4 and S8 were assayed via immunoblot.

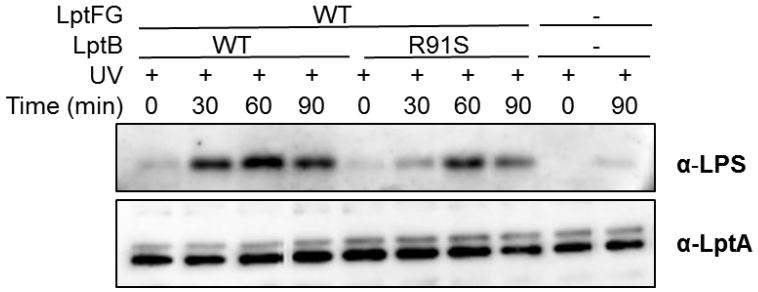

Figure S9. The activity of LptB(R91S) is similar to wild-type LptB *in vitro*. Top) Time-course of LPS release to LptA(I36*p*BPA) from RSO vesicles containing $LptB_2FGC$ with wild-type LptB or LptB(R91S). Accumulation of the cross-linked LptA-LPS adduct is dependent on overexpression of inner membrane Lpt proteins.

Materials and Methods

E. coli strain Nova Blue [*endA1 hsdR17* (r_{K12}^{-} m_{K12}^{+}) *supE44 thi-1 recA1 gyrA96 relA1 lac* F′[*proA*$^{+}$*B*$^{+}$*lacI*^{q}*ZΔM15*::Tn*10*] (Tet^{R})] from Novagen was used for plasmid manipulations. *E. coli* strain KRX [F′, *traD36, ΔompP, proA*$^{+}$*B*$^{+}$, *lacI*^{q}, *Δ(lacZ)M15] ΔompT, endA1, recA1, gyrA96 (Nal*^{r}*), thi-1, hsdR17* (r_K^{-}, m_K^{+}), *e14*$^{-}$ *(McrA*$^{-}$*), relA1, supE44, Δ(lac-proAB), Δ(rhaBAD)::T7 RNA polymerase*] from Promega was used for protein purification. *E. coli* strain BL-21(λDE3) [*F- ompT gal dcm lon hsdSB(rB–, mB–) λ(DE3)*] from Novagen was used for right-side-out vesicle preparation. Other strains used in this study are listed in Table S2.

The *lptB1* mutant was isolated serendipitously while attempting to add the codons for a C-terminal sequence containing a poly-histidine tag immediately upstream of the stop codon of chromosomal *lptB*. Primers 5HisTagP1 and P2 were used to amplify a kanamycin-resistance cassette using pKD4 (4) as a template in PCR. The resulting amplified sequence was then used as a template in another PCR using the 5LptBhis and 3LptBP2 primers. The resulting PCR product was flanked by regions of homology to the site of insertion in the *lptB* chromosomal locus. Insertion of the recombinant DNA into strain DY378 was accomplished using recombineering and selecting for kanamycin resistance (5). The *lptB* locus was then amplified from kanamycin-resistant recombinants using primers 5LptB77Up and 3LptBDOWN in PCR. Sanger DNA sequencing of the resulting PCR product from one of the recombinants revealed that a 5-bp deletion had occurred immediately after the last codon of wild-type *lptB* and within the sequence encoding the tag. This deletion resulted in a frameshift that causes the addition of a 34-residue sequence (ISPSPSPYGSGPEAKCRLELLRSSYSLESIGTSE) after the last amino acid of LptB instead of the desired tag. The mutant allele, which was named *lptB1*, was then introduced into strain NR754 using P1vir transduction and selecting for kanamycin-resistant transductants. Analysis of a transductants demonstrated that *lptB1* confers sensitivity to a wide range of antibiotics. One such transductant, NR1768, was used in this study.

The plasmids used in this study are listed in Table S3. Point mutations in pCDFduet-LptB-LptFG were introduced by site-directed mutagenesis using the oligonucleotides listed in Table S4. PCR amplification was performed with KOD Hot Start DNA polymerase from Novagen. Restriction enzyme DpnI was purchased from New England Biolabs. All other materials were purchased from Sigma Aldrich unless noted otherwise.

Name	Description	Ref.
NR754	MC4100 *ara*$^{+}$	(6)
NR1250	NR754 Δ*tolC::frt*	This study
NR1768	NR754 *lptB1-kan*	This study
NR1962	NR754 *lptB1/G33C-kan*	This study
NR1963	NR754 *lptB1/R144H-kan*	This study
NR2761	NR754 Δ*lptFG::frt* (pBAD18LptFG3)	(7)
NR3327	NR754 Δ*lptFG::frt* (pBAD18LptFG3/LptFE84A/LptGE88A)	(7)
NR3602	NR754 *tet2 lptBR91S*	(7)
NR4127	NR754 *tet2 lptBR91S* Δ*lptFG::frt* (pBAD18LptFG3/LptFE84A/LptGE88A)	(7)

Table S2. Strains used in this study

Name	Description	Ref.
pET22/42-LptB-His_8	Encodes LptB with a C-terminal His_8 tag	(8)
pBAD/HisA-LptC	Encodes LptC for the RSO vesicle assay	(9)
pCDFduet-LptB-LptFG	Encodes LptB and LptFG for the RSO vesicle assay	(9)
pET2 2b-LptA(I36Am)-His	LptA with amber codon (TAG) for substitution with *p*BPA	(9)
pSup-BpaRS-6TRN	Encodes amino-acyl tRNA synthetase as well as tRNAs for incorporation of *p*BPA at TAG codons	(10)

Table S3. Plasmids used in this study

Name	Sequence (5’ to 3’)
5HisTagP1	AGA GGA TCT CAC CAT CAC CAT CAC CAT ACG GAT CCG GCC CTG AGG CTA AGT GTA GGC TGG AGC TGC TTC

P2	CAT ATG AAT ATC CTC CTT A
5lptBhis	CGG CAC GCC TAC AGA AAT CTT ACA AGA CGA ACA CGT TAA GCG TGT ATA CCT TGG GGA AGA CTT CAG ACT CAG AGG ATC TCA CCA TCA CCA
3lptBP2	CTG AGT TGC AAA CCT TGC TTC ATG TTC AGA ATC GTA CTC TCC TGC TAA AAC GTC GCA AAC TTC TAC CCT ACA TAT GAA TAT CCT CCT TA
5LptB77UP	GTT CTG GTG CCG TCG CAG
3LptB50down	CAT GTT CAG AAT CGT ACT CTC CTG C
LptF_E84A_f	GGC AAA CTG TAT ACC GAA AGT GCG ATT ACG GTA ATG CAT GCC TGC GGC C
LptF_E84A_r	GGC CGC AGG CAT GCA TTA CCG TAA TCG CAC TTT CGG TAT ACA GTT TGC C
LptG_E88A_f	GGG ATG CTG GCG CAG CGC AGC GCG CTG GTG GTG ATG CAG GCT TCT GG
LptG_E88A_r	CCA GAA GCC TGC ATC ACC ACC AGC GCG CTG CGC TGC GCC AGC ATC CC
LptB_R91S_f	CTG CCA CAG GAA GCC TCC ATT TTC AGC CGC CTC AGC GTT TAC GAT AAC CTG
LptB_R91S_r	CAG GTT ATC GTA AAC GCT GAG GCG GCT GAA AAT GGA GGC TTC CTG TGG CAG

Table S4. Oligonucleotides used in this study

Disk diffusion assay

Disk diffusion assays were performed as described in ref. (11). Premade Sensi-Disc (BD-Beckton, Dickinson and Company) were used for bacitracin 10IU, erythromycin 15 μg, novobiocin 30 μg, and rifampin 5 μg. When needed, disks of nalidixic acid (10 μg if unnoted or 5 μg when noted), novobiocin (5 μg) and novobiocin-adamantyl (5 μg) were prepared by soaking into sterile 7 mm disks hole-punched from Whatman grade:17chr chromatography paper.

For assessing the effect of novobiocin on outer membrane permeability, disk diffusion assays were performed with LB Miller plates (1.5 % agar) and LB Miller top agar (0.75 % agar) either without novobiocin or containing 0.2, 2, and 20 μM.

Efficiency of plating assay

Efficiency of plating assays were performed on indicated media using the method described in ref. (12).

LptB-His overexpression and purification for crystallography

LptB-His (full-length LptB with a C-terminal His_8 tag) was purified as described in ref. (11) with minor modifications. Overnight cultures of KRX cells (Promega) transformed with plasmid pET22/42-LptB-His_8 were diluted 100x into LB Miller media containing 50 μg/mL carbenicillin. Cultures were grown at 37 °C, 220 rpm to OD 0.8, at which point the temperature was reduced to 16 °C. Following 30 min of shaking at 16 °C, overexpression was induced with 0.2% L-rhamnose monohydrate. Cultures were grown at 16 °C, 220 rpm for 14 h.

Cells were harvested by centrifugation at 5000 x g, 4 °C for 20 min. Pellet was resuspended in Buffer A: Tris-buffered saline (TBS; 20 mM Tris [pH 8.0], 150 mM NaCl), 20% (vol/vol) glycerol, and 0.5 mM Tris(3-hydroxypropyl)phosphine (THP: EMD Milipore). To facilitate lysis, 0.5 mM phenylmethylsulfonyl fluoride (PMSF), 50 μg/mL lysozyme, and 50 μg/mL DNAse I were added to the cell suspension. Cells were lysed 3x through a high-pressure cell disruptor. Unbroken cells were removed by centrifugation at 6000 xg, 4 °C for 10 min. To pellet membranes, cell lysate was centrifuged at 100,000 x g, 4 °C for 30 min. Membranes were discarded and 10 mM imidazole was added to the supernatant.

In preparation for nickel affinity chromatography, Ni-NTA Superflow resin (Qiagen) was washed with water and equilibrated with Buffer A supplemented with 10 mM imidazole. Cell lysate supernatant was incubated with equilibrated Ni-NTA resin at 4 °C for 1 h with gentle rocking. Following incubation, flow-through was removed and resin was washed with 20 column volumes of Buffer A with 20 mM imidazole. Protein was eluted in one batch with 2.7 column volumes of Buffer A with 200 mM imidazole. Eluate was concentrated in a 10-kDa molecular weight cut-off (MWCO) centrifugation filter (Amicon; Millipore) to ~50 mg/mL and flash frozen.

Protein was further purified by size exclusion chromatography on Superdex 200 10/30 GL column in Buffer A. Fractions containing protein were pooled and concentrated in a 10-kDA MWCO centrifugation filter to ~50 mg/mL. Protein aliquots were flash-frozen and stored at -80 °C. Protein concentration was measured using the Biorad DC protein assay.

LptB-His crystallization and novobiocin soak

LptB-His was crystallized using conditions described in ref. (11). Purified LptB-His was diluted into Buffer A to a concentration of 20 mg/mL. The 20 mg/mL stock was diluted 2x into TBS, yielding a final protein concentration of 10 mg/mL and glycerol concentration of 10%. This solution was incubated with 2.5 mM ATP and 2.5 mM $MgCl_2$ for 1 h on ice before setting up drops.

Crystals were grown by vapor diffusion in hanging drops at room temperature. 1 μL protein solution was mixed with 1 μL reservoir solution consisting of 100 mM MES (pH 6.5) and 30% (wt/vol) PEG 4000. As observed in ref. (11), flat, triangular crystals appeared after several days.

For the novobiocin soaks, crystals were transferred to 2-μL drops of reservoir solution (100 mM MES (pH 6.5), 30% PEG 4000) containing 2.5 mM novobiocin sodium salt. Crystals were soaked for ~90 min at room temperature and then flash-frozen in cryoprotectant containing 100 mM MES (pH 6.5), 33% PEG 4000, 24% glycerol, and 2.5 mM novobiocin.

LptB-His co-crystallization with novobiocin-adamantyl

LptB-His was crystallized using conditions described above. The 20 mg/mL stock was diluted 2x into TBS, yielding a final protein concentration of 10 mg/mL and glycerol concentration of 10%. This solution was incubated with 2.5 mM ATP, 2.5 mM $MgCl_2$ for 1 h on ice before setting up drops.

Crystals were grown by vapor diffusion in hanging drops at room temperature. 1 μL protein solution was mixed with 1 μL reservoir solution consisting of 100 mM MES (pH 6.5), 30% (wt/vol) PEG 4000, and 1.3 mM novobiocin-adamantyl solution (final droplet [DMSO] = 7%). As observed in ref. (11), flat, triangular crystals appeared after several days. Crystals were flash-frozen in cryoprotectant containing 100 mM MES (pH 6.5), 33% PEG 4000, 24% glycerol, and 2.5 mM novobiocin-adamantyl.

Crystallography data collection

The X-ray diffraction data for the LptB-ADP-NOV and LptB-ADP-ADN crystals were collected at 0.97918 Å at beamline 24-ID-E of the Advanced Photon Source at Argonne National Laboratory. LptB-ADP-NOV and LptB-ADP-ADN belong to the space group *C*121.

Crystallography data processing and structure determination

The LptB-ADP-NOV dataset was indexed and integrated using iMosflm (13) and scaled using the CCP4 (14) program AIMLESS (15). The structure was solved by molecular replacement with Phaser (16) using the complete LptB-ADP structure from ref. (11) as a search model (PDB: 4P32). Initial rounds of refinement in Phenix (17-19) were performed with rigid body refinement, simulated annealing, and ADP (atomic displacement parameter or *B*-factor) refinement, yielding a model with R_{free} and R_{work} values of 29.9% and 25.0%, respectively. This model contained clear unassigned density at the LptB dimer interface.

Following manual placement of novobiocin into the unassigned density in COOT (20), the model was further refined in Phenix with cycles of minimization, simulated annealing, and ADP refinement, interspersed with manual editing in COOT. Waters and magnesium ions were placed, and the refinement was completed using cycles of minimization, ADP refinement, and translation/libration/screw (TLS) refinement with TLS parameters from the TLS motion determination server (21). Ligand restraints were generated using the Mogul geometry optimization in eLBOW (22), and coordination sphere restraints were generated with ReadySet (19). The R_{free} and R_{work} values for the final LptB-ADP-NOV structure are 22.0% and 17.9%, respectively.

The LptB-ADP-ADN dataset was processed with the same procedure as the LptB-ADP-NOV dataset, except that an adamantyl group was modeled in to fit the electron density. The R_{free} and R_{work} values for the final LptB-ADP-ADN structure are 22.4% and 18.0%, respectively.

Much of the software used in this project was installed and configured by SBGrid (23). Figures were prepared using Pymol (24).

Table S5. Data collection and refinement statistics

Data Set	LptB-ADP-NOV	LptB-ADP-ADN
Space group	C121	C121
Unit cell		
Dimensions (a, b, c), Å	190.32, 35.10, 63.05	104.03, 34.78, 62.71
Angles (α, β, γ), °	90.00, 91.52, 90.00	90.00, 101.38, 90.00
Data collection*		
Wavelength, Å	0.97918	0.97918
Resolution range, Å	63.03-2.00 (2.05-2.00)	43.71-1.95 (2.02-1.95)
R_{merge}	0.128 (0.622)	0.068 (0.587)
Completeness, %	99.4 (99.2)	99.2 (98.9)
Mean $I/\sigma(I)$	8.7 (2.1)	9.56 (1.95)
Unique reflections	28,485	16,230
Multiplicity	3.5 (3.5)	1.9 (1.9)
Refinement*		
R_{work}, %/R_{free}, %	17.94/22.03	18.01/22.36
No. of LptB molecules per asymmetrical unit	2	1
No. of modeled LptB residues per chain	234 (A)/226 (B)	233 (A)
No. of water molecules	101	105
No. of ions	2	1
Average *B*-factor, Å^2		
Protein	20.61	33.98
Ligands	18.26	43.42
Solvent	17.76	37.10
Ramachandran plot		
Favored, %	98.9	98.27
Disallowed, %	0	0
rmsd from ideal geometry		
Bond lengths, Å	0.007	0.004
Bond angles, °	0.747	0.72

*Values in parentheses are for the shell with the highest resolution.

Minimum inhibitory concentration assay

Strains were grown overnight in LB Miller broth shaking at 220 rpm at 37 °C. Overnight cultures were diluted 1:1,000 (v/v) in LB Miller and 100 μL of diluted culture were added to each well of a 96-well plate. To the first well of each row (column no. 1) of this plate, an additional 100 μL of mixed diluted culture and test compound were added to a final concentration of 500 μM. A 100-μL aliquot was serially transferred across rows starting from column no. 1 to column no. 11. Wells in column no. 12 did not receive any test compound. After incubating the plate at 37 °C overnight (~16 h), turbidity (OD_{600}) was measured using a Spectramax 384 Plus plate reader (Molecular Devices) or an xMark™ microplate spectrophotometer (Bio Rad). The minimum inhibitory concentration (MIC) was defined as the lowest concentration of compound needed to completely inhibit bacterial growth.

Gyrase activity assay

The *Escherichia coli* gyrase supercoiling inhibition assay kit was purchased from the Inspiralis company (Norwich, UK). The assay was conducted according to the provided instructions. 1 U of DNA gyrase was incubated with 0.5 μg of relaxed pBR322, and the stated compound concentration, in a reaction volume of 30 μL at 37 °C for 30 minutes in Assay Buffer (35 mM Tris•HCl, pH 7.5; 24 mM KCl; 4 mM $MgCl_2$, 2 mM DTT, 1.8 mM spermidine, 1 mM ATP, 6.5% (w/v) glycerol, 0.1 mg/mL albumin). The supercoiling reactions were quenched by the addition of 30

μL of STEB buffer (40% (w/v) sucrose, 100 mM Tris•HCl pH 8, 10 mM EDTA, 0.5 mg/mL bromophenol blue) and 30 μL of chloroform/isoamyl alcohol (v/v, 24:1). Samples were vortexed for 5 minutes and centrifuged at max speed for 1 minute. 20 μL of the upper aqueous layer were loaded on a 1 % (w/v) agarose gel free of DNA intercalator and run at 85 V for 2 h. The gel was then stained with DNA intercalator and visualized with an Azure imaging system.

Right-side out vesicle preparation

Right-side out (RSO) vesicles were prepared as described in ref. (7) with minor modifications. BL-21(λDE3) *E. coli* were transformed with plasmid pBAD18HisA-LptC along with one of pCDFduet (empty vector), pCDFduet-LptB-LptFG (encoding wild-type *E. coli* proteins), pCDFduet-LptB-LptFG(ch) (encoding wild-type LptB and LptF(E84A)LptG(E88A)) or pCDFduet-LptB(R91S)-LptFG. Overnight cultures were diluted 1:100 into 50 mL of LB Miller media containing 50 μg/mL carbenicillin and 50 μg/mL spectinomycin and grown at 24 °C to OD_{600} ~ 1. Growth temperature was then increased to 37 °C and expression induced by addition of 0.02% arabinose and 10 μM Isopropyl β-D-1-thiogalactopyranoside (IPTG). After two hours, cells were pelleted, resuspended in 5 mL 50 mM Tris-HCl (pH 7.4) 250 mM sucrose, 300 μg/mL lysozyme and 150 μg/mL DNaseI, and converted to spheroplasts by drop-wise addition of 5 mL buffer containing 50 mM Tris-HCl (pH 7.4), 250 mM sucrose and 3 mM EDTA followed by incubation on ice for 30 minutes.

To convert spheroplasts to RSO-vesicles, spheroplasts were pelleted, 6000 *g* x 10 minutes, resuspended in 5 mL lysis buffer (20 mM Tris (pH 8), 150 mM NaCl, 0.1 mM EDTA, 5 mM $MgCl_2$, and 5 mM sodium-ATP (pH ~7)), pelleted at 10,000 *g* x 15 minutes, and resuspended in the supernatant to complete lysis. RSO-vesicles were collected by centrifugation at 200,000 *g* x 30 minutes and resuspended in 1 mL of 10% v/v glycerol, 20 mM Tris (pH 8.0), 150 mM NaCl, 5 mM $MgCl_2$, and 5 mM sodium-ATP (pH ~7). Total protein concentration in RSO-vesicle samples was determined by DC-protein assay (BioRad), and samples were either used immediately in LPS release assays or flash-frozen and stored at -80 °C.

Purification of LptA* (LptA(I36*p*BPA))

LptA* was purified as described in ref. (7) with minor modifications. BL-21(λDE3) *E. coli* containing pSup-BpaRS-6TRN and pET22b-LptA(I36Am) were grown to OD_{600} ~ 0.6 at 37 °C in 1.5 L LB Miller media containing 50 μg/mL carbenicillin, 30 μg/mL chloramphenicol and 0.7 mM *para*-benzoylphenylalanine (*p*BPA, BaChem), and induced for 2 hours with 50 μM IPTG. These cells were pelleted, converted to spheroplasts as described above, and the spheroplasts pelleted at 6000 *g* x 10 minutes. Supernatant from the spheroplasts was collected and supplemented with 1 mM PMSF and 10 mM imidazole, and clarified by ultracentrifugation at 100,000 *g* x 30 minutes. Supernatant was applied twice to Ni-NTA resin, washed with 2 x 20 column volumes of wash buffer (20 mM Tris (pH 8.0), 150 mM NaCl, 10% v/v glycerol) with 20 mM imidazole, and eluted with 2 x 2.5 column volumes of wash buffer with 200 mM imidazole. Eluate was concentrated to ~1 mg/mL using an Amicon 10 kDa cut-off Amicon centrifugal filter (Millipore), aliquoted, and stored at -80 °C.

LPS-release assay

The *in* vitro LPS-transport experiments in Figures 4b, 4c, and S8 were set-up as described in ref. (7) with some modifications. RSO-vesicles (50 μg total protein) were diluted into 100 μL reaction buffer (10% v/v glycerol, 20 mM Tris (pH 8.0), 150 mM NaCl, 5 mM sodium-ATP, 5 mM $MgCl_2$), and incubated on ice with novobiocin, adamantyl-novobiocin, or no compound for 15 minutes (50x compound stocks in water were used for each concentration). To start the assay, 3 μg of LptA* was added to each sample, with each time-point its own 100 μL sample, and samples were then incubated at 30 °C for the stated time. To cross-link LptA* to LPS, samples were transferred to a 96-well plate and irradiated with 365 nm UV-light for 5 minutes. Cross-linked samples were then mixed 1:1 with 2x SDS loading dye (100 mM Tris-HCl pH 6.8, 4% w/v SDS, 0.05% w/v bromothymol blue, 20% glycerol) with 5% β-mercaptoethanol, and boiled for 10 minutes.

Immunoblotting was used to assess LptA*-LPS levels in each sample. Boiled samples were run on home-made 4%/15% polyacrylamide stacking gels at 0.02 A constant-current until the 15 kDa ladder band (BioRad Precision Plus all Blue standards) had run out of the gel, transferred to PVDF, and immunoblotted with mouse anti-LPS core antiserum (HyCult Biotechnology) followed by sheep-anti-mouse IgG horseradish peroxidase conjugate (GE Healthcare). LptA levels were assessed similarly, using rabbit anti-LptA antiserum (25) followed by donkey anti-rabbit

horseradish peroxidase conjugate (GE Amersham). ECL Prime Western Blotting Detection Reagent (GE Amersham) was used to visualize antibody-label bands in conjunction with an Azure c400 imaging system (Azure Biosystems).

To assess the expression levels of inner-membrane Lpt components in the different RSO preparations, samples from LPS release assays were also subject to SDS-PAGE and immunoblotting as described above. Rabbit anti-LptC (25), rabbit anti-LptF (26), or rabbit anti-LptB (11) antisera were used to label Lpt proteins on PVDF and in turn detected and imaged as described for LptA.

Fbn–LptB binding assay

5 mL of the buffered **Fbn** ligand solution was prepared by mixing 200 μL of 25X TBS pH 8.0, 125 μL 200 mM ADP pH 7.0, 125 μL 200 mM $MgCl_2$, 4.43 μL of 56.5 mM **Fbn**, 4.55 mL of D_2O. Final [Tris-Cl] = 50 mM, [NaCl] = 150 mM, [ADP] = 5 mM, [$MgCl_2$] = 5 mM, [**Fbn**] = 50 μM. In ten 1.5 mL Eppendorf tubes, on ice, the corresponding volume of stock LptB-His protein was added to the buffered **Fbn** solution. The tubes were vortexed briefly, the solutions transferred to Bruker Biospin 5.0x103.5 mm NMR tubes (for SampleJet) and stored at +4 °C until acquisition. Data were acquired using a Bruker 500 MHz Avance III with multi-nuclear smart probe operating at a frequency of 470.5453180 MHz for ^{19}F and 500.1320005 MHz for ^{1}H. A standard fluorine 1D pulse program with proton decoupling was used; temperature (T) = 298.1 K, number of scans (NS) = 3072, relaxation delay (D1) = 0.75 s, pulse angle = 70 °. After acquisition, FIDs were Fourier transformed, phased, and processed with the exponential multiplication window function (LB = 3.00 Hz) in MestReNova MNova v10. The ^{19}F linewidths were plotted against log [LptB] in GraphPad Prism 7 software using the nonlinear fit log(agonist) vs. response model, variable slope (four parameters).

General synthetic methods

Unless otherwise noted, all reactions were performed under anhydrous N_2. Solvents were purchased in Sure-Seal bottles from Sigma-Aldrich and used without further purification. Thin layer chromatography (TLC) was carried out using EM Science silica gel 60 F254 plates; the developed plate was analyzed by UV lamp (254 nm). Column chromatography was performed with the Teledyne-Isco CombiFlash R_f 200 system using pre-packed silica gel column cartridges and hexanes/ethyl acetate or dichloromethane/methanol as the solvent system. ^{1}H NMR and ^{13}C NMR spectra were recorded in DMSO-*d*6 or $CDCl_3$ on a Varian Inova-500 MHz spectrometer unless otherwise noted. Chemical shifts are reported in ppm with the residual solvent signal as the reference, and coupling constants (*J*) are given in hertz. The peak information is described as: br = broad singlet, s = singlet, d = doublet, t = triplet, q = quartet, m = multiplet. The molar ratio of isolated imine geometric isomers was determined by NMR spectroscopy. High-resolution mass spectra (HRMS) were performed on a Bruker microTOFII ESI LCMS system mass spectrometer using sodium formate as the standard. Novenamine and *N*-acylated derivatives were obtained by existing literature methods (27).

Synthesis of novobiocin-adamantyl (adn)

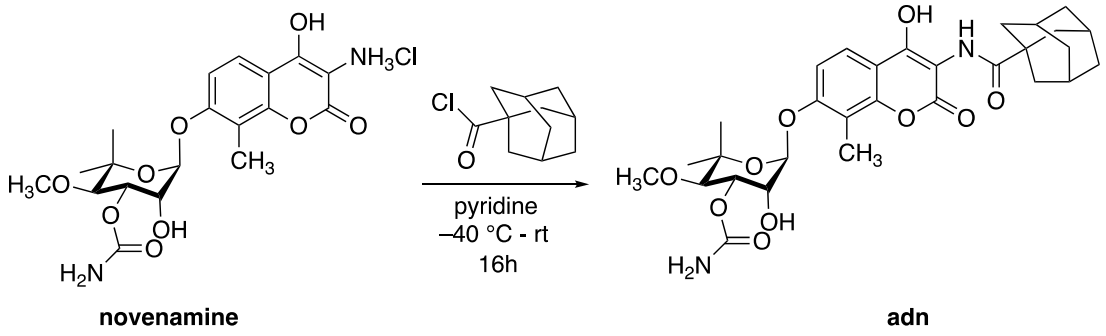

novenamine **adn**

Novenamine hydrochloride (40 mg, 0.09 mmol, 1.0 eq.) and a magnetic stirbar were added to a 25 mL conical flask and sealed with a rubber septum. A vent needle was inserted and the flask was sparged with N_2 for 5 minutes (**free novenamine begins to oxidize upon exposure to O_2!).** 2 mL of pyridine were added under positive N_2 pressure and the flask was cooled to –40 °C in a dry ice/acetonitrile bath. 1-adamantanecarbonyl chloride (17.2 mg, 0.09 mmol, 1.0

eq.) was dissolved in 0.5 mL of pyridine and added to the stirring novenamine solution. The solution was stirred for 16 h while allowing the bath to warm to room temperature. The reaction mixture was concentrated by rotary evaporation and then subjected to flash column chromatography with DCM/MeOH (10 mg, 16% isolated yield). The product was further purified by reversed-phase column chromatography with a Zorbax C18 column with acetonitrile/water as the eluent (90% MeCN to 100% MeCN over the course of 15 minutes), and the final product was obtained as a white solid (6.7 mg, 13% isolated yield).

Synthesis of fluorobiocin (fbn)

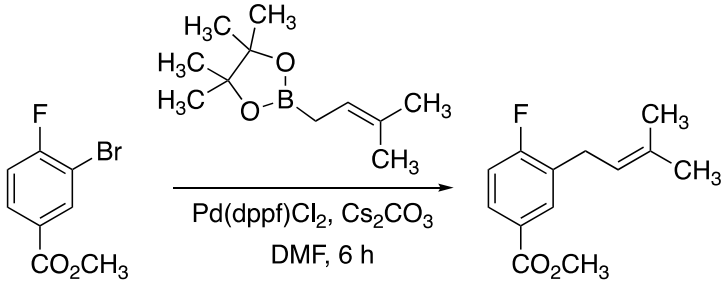

Methyl 3-bromo-4-fluorobenzoate (500 mg, 2.1 mmol, 1.0 eq.), palladium catalyst (314 mg, 0.43 mmol, 20 mol %), Cs_2CO_3 (1.4 g, 4.3 mmol, 2.0 eq.) were charged in a 100 mL round bottom flask. 20 mL of anhydrous DMF and a magnetic stirbar were added and the flask was sealed with a rubber septum. A vent needle was inserted and the flask was sparged with N_2 for 5 minutes. 3-methyl-2-butenylboronic acid pinacol ester (951 μL, 4.3 mmol, 2.0 eq.) was added and the reaction was heated to 90 °C under positive N_2 pressure for 6 h. The reaction mixture was cooled to room temperature and filtered through a pad of Celite rinsed with EtOAc. 100 mL of water were added and the product was extracted by washing with 3 x 50 mL ethyl acetate. The organic layer was washed several times with water, saturated sodium chloride, and then dried over sodium sulfate. Following filtration, the extract was concentrated by rotary evaporation and subjected to flash column chromatography (hexanes/EtOAc) to afford methyl 4-fluoro-3-(3-methylbut-2-en-1-yl)benzoate as an oil (50% isolated yield), which was used immediately in the next step.

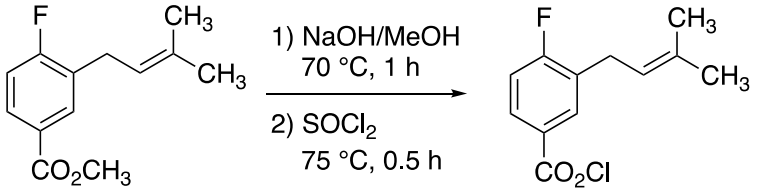

Methyl 4-fluoro-3-(3-methylbut-2-en-1-yl)benzoate (220 mg, 1 mmol) was added to a 15 mL scintillation vial equipped with a magnetic stirbar. 2 mL of 1M NaOH in methanol and a few drops of water were added to the vial. The reaction was heated to 70 °C for 1 h. The carboxylate product precipitated upon completion of the reaction, and the mixture was concentrated by rotary evaporation. The carboxylate salt was protonated by the dropwise addition of 1M HCl. Ethyl acetate (5 mL) and water (5 mL) were added and the acid product was extracted from the organic layer. The extract was dried over sodium sulfate, filtered, and concentrated by rotary evaporation. The carboxylic acid product was a white solid and was used without further purification. Thionyl chloride (700 μL, 14 eq.) was added and the mixture was heated to 75 °C for 0.5 h. The leftover thionyl chloride was removed by rotary evaporation and 150 mg of a sticky orange gel (88% isolated yield).

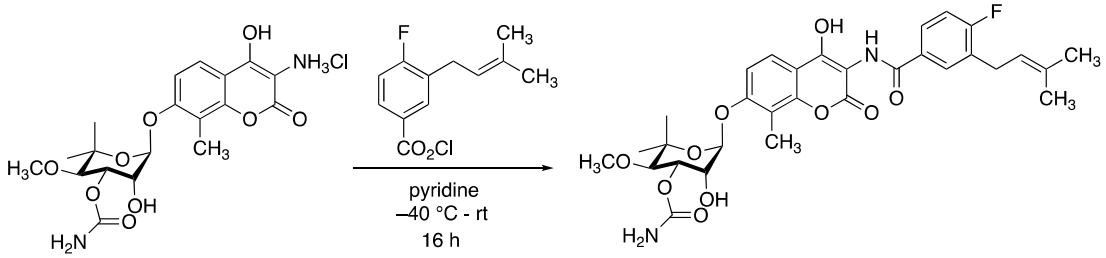

novenamine **fbn**

Novenamine hydrochloride (118 mg, 0.26 mmol, 1.0 eq.) and a magnetic stirbar were added to a 25 mL conical flask and sealed with a rubber septum. A vent needle was inserted and the flask was sparged with N_2 for 5 minutes (**free novenamine begins to oxidize upon exposure to O_2!).** 2 mL of pyridine were added under positive N_2 pressure and the flask was cooled to –40 °C in a dry ice/acetonitrile bath. 4-fluoro-3-prenylbenzoyl chloride (75 mg, 0.31 mmol, 1.2 eq.) was dissolved in 0.5 mL of pyridine and added to the stirring novenamine solution. The solution was stirred for 16 h while allowing the bath to warm to room temperature. The reaction mixture was concentrated by rotary evaporation and then subjected to flash column chromatography with DCM/MeOH. The product was further purified by reversed phase column chromatography with a Zorbax C18 column with acetonitrile/water as the eluent (90% MeCN to 100% MeCN over the course of 15 minutes), 12.7 mg (8% isolated yield after semi-preparative HPLC).

Characterization and NMR spectra

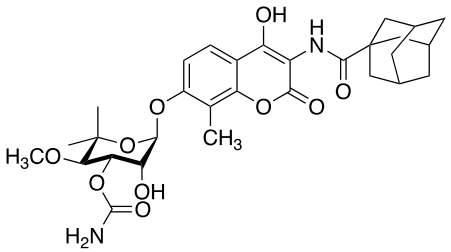

1-adamantyl-novobiocin (adn)

(3*R*,4*S*,5*R*,6*R*)-6-((3-((3*R*,5*S*)-adamantane-1-carboxamido)-4-hydroxy-8-methyl-2-oxo-2*H*-chromen-7-yl)oxy)-5-hydroxy-3-methoxy-2,2-dimethyltetrahydro-2*H*-pyran-4-yl carbamate

(1-adamantyl novobiocin, "adn"). White solid; TLC R_f = 0.4 (5% MeOH/DCM); ^{1}H NMR (400 MHz, DMSO-d_6) δ 8.21 (s, 1H), 7.70 (d, *J* = 8.8 Hz, 1H), 7.10 (d, *J* = 9.1 Hz, 1H), 6.62 (d, *J* = 61.5 Hz, 2H), 5.58 (s, 1H), 5.50 (d, *J* = 2.4 Hz, 1H), 5.15 (dd, *J* = 9.7, 3.1 Hz, 1H), 4.07 (d, *J* = 3.0 Hz, 1H), 3.49 – 3.44 (m, 4H), 3.23 (br, 1H), 2.19 (s, 3H), 1.99 – 1.91 (m, 3H), 1.90 – 1.84 (m, 6H), 1.69 – 1.56 (m, 6H), 1.25 (s, 3H), 1.04 (s, 3H); ^{13}C NMR (101 MHz, DMSO-d_6) δ 177.9, 163.1, 160.6, 156.5, 156.3, 150.6, 122.0, 112.5, 111.7, 109.6, 100.9, 98.4, 80.8, 78.0, 70.3, 68.8, 61.0, 40.4, 38.4, 36.1, 28.5, 27.6, 22.7, 8.3; HRMS (ESI Neg) *m/z* calculated for $C_{30}H_{37}N_2O_{10}$ $[M–H]^-$ 585.2454, found: 585.2471.

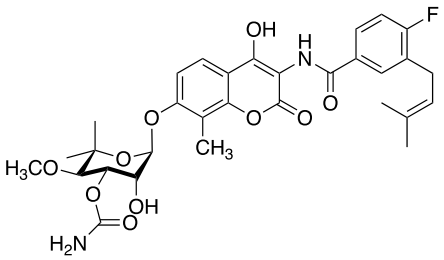

fluorobiocin (fbn)

(3*R*,4*S*,5*R*,6*R*)-6-((3-(4-fluoro-3-(3-methylbut-2-en-1-yl)benzamido)-4-hydroxy-8-methyl-2-oxo-2*H*-chromen-7-yl)oxy)-5-hydroxy-3-methoxy-2,2-dimethyltetrahydro-2*H*-pyran-4-yl carbamate (fluorobiocin, "fbn"). White solid; TLC R_f = 0.5 (10% MeOH/DCM); ^{1}H NMR (500 MHz, DMSO-d_6) δ 12.5 (br, 1H), 9.3 (s, 1H), 7.9 – 7.8 (m, 2H), 7.6 (d, *J* = 8.8 Hz, 1H), 7.2 (t, *J* = 9.1 Hz, 1H), 7.1 (d, *J* = 8.9 Hz, 1H), 6.8 – 6.5 (m, 2H), 5.6 (d, *J* = 5.2 Hz, 1H), 5.5 (d, *J* = 2.5 Hz, 1H), 5.3 (t, *J* = 7.5 Hz, 1H), 5.2 (dd, *J* = 9.9, 3.1 Hz, 1H), 4.1 – 4.0 (m, 1H), 3.5 – 3.5 (m, 4H), 3.3 (d, *J* = 7.5 Hz, 2H), 2.2 (s, 3H), 1.7 – 1.7 (m, 6H), 1.3 (s, 3H), 1.1 (s, 3H); ^{13}C NMR (126 MHz, DMSO-d_6) δ 165.4, 162.1 (d, *J* = 248.8 Hz), 161.8 (br), 160.8, 156.7, 156.3, 150.9, 132.8, 130.5 (d, *J* = 5.8 Hz), 130.3 (d, *J* = 2.5 Hz), 127.9 (d, *J* = 8.8 Hz), 127.7 (d, *J* = 16.9 Hz), 121.9, 121.2, 114.8 (d, *J* = 22.8 Hz), 112.5, 111.0, 109.5, 100.1, 98.5, 80.7, 78.0, 70.3, 68.8, 61.0, 28.5, 27.0, 25.5, 22.7, 17.6, 8.3; ^{19}F NMR (471 MHz, DMSO-d_6) δ -114.6; HRMS (ESI Neg) *m/z* calculated for $C_{31}H_{34}FN_2O_{10}$ $[M–H]^-$ 613.2197, found: 613.2199.

^{1}H NMR of novobiocin-adamantyl (adn)

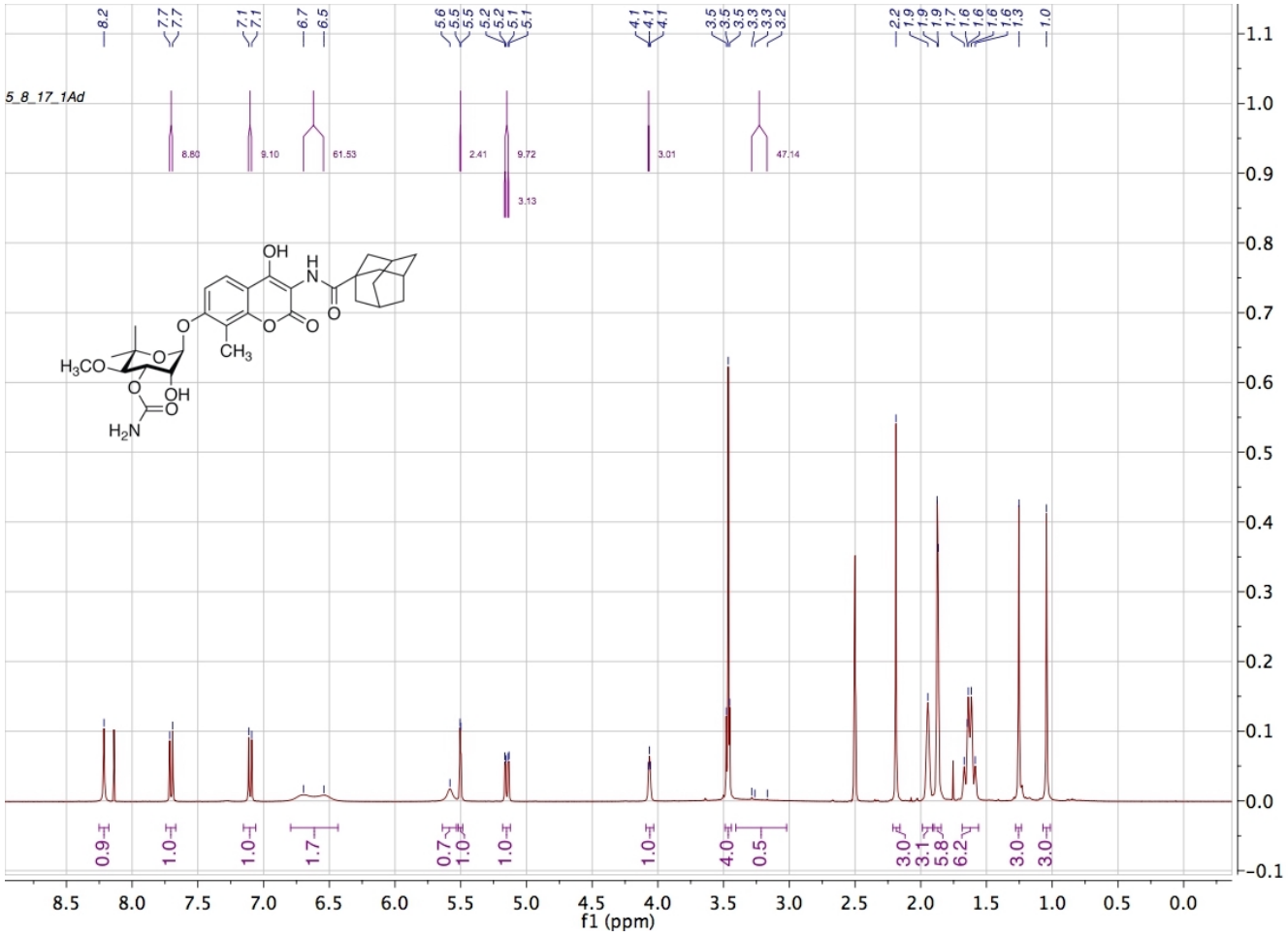

^{13}C NMR of novobiocin-adamantyl (adn)

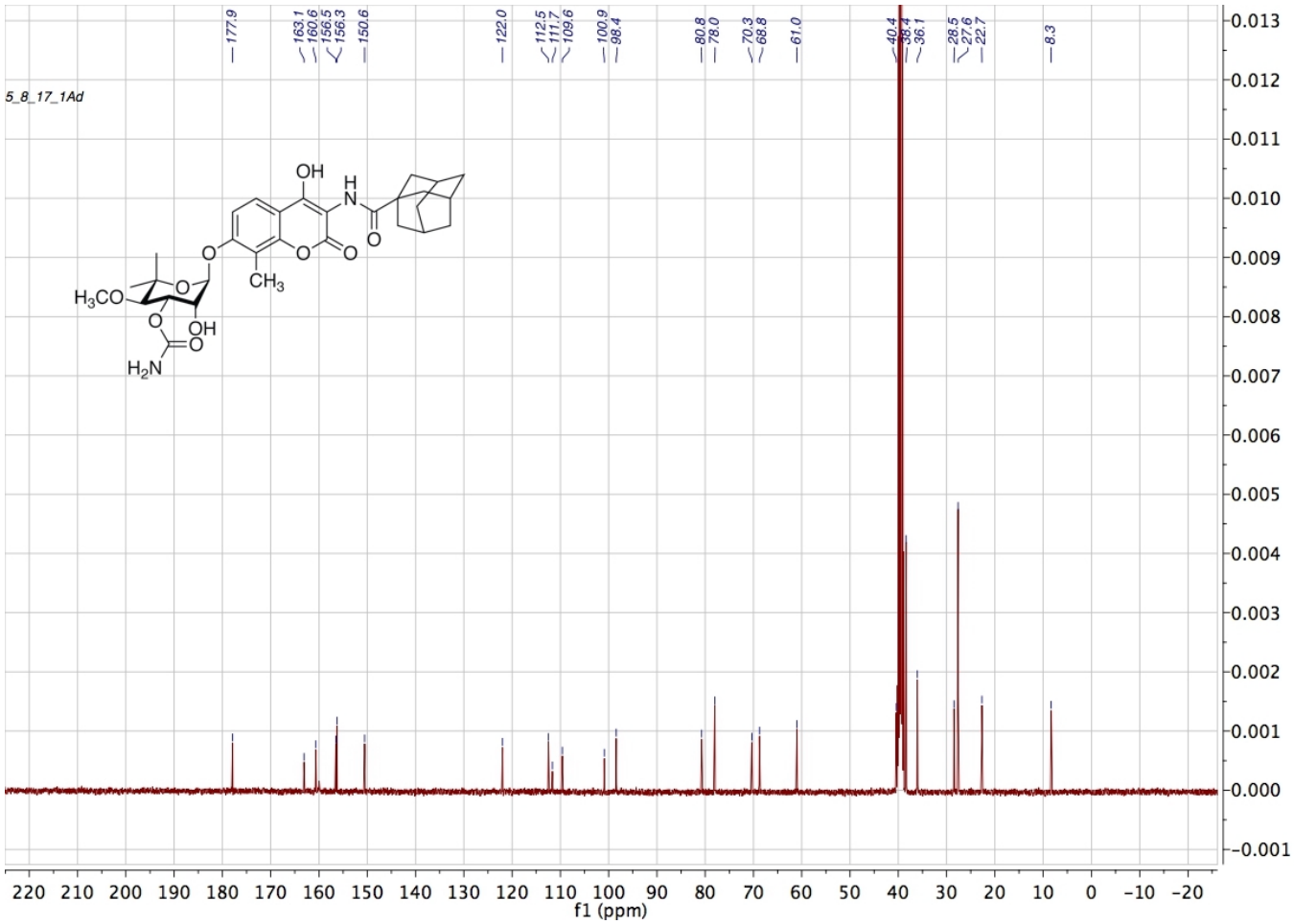

^{1}H NMR of fluorobiocin (fbn)

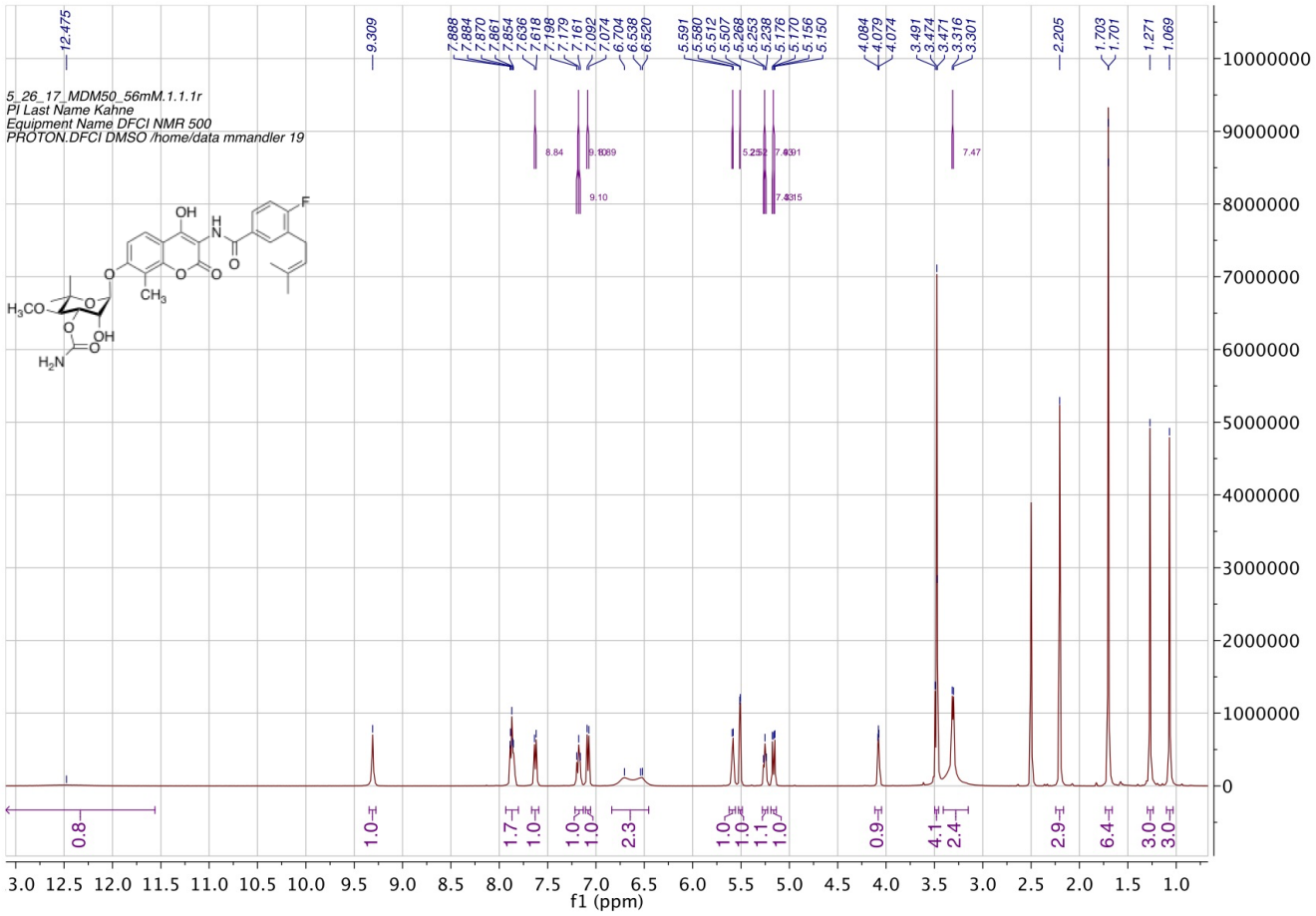

^{13}C NMR of fluorobiocin (fbn)

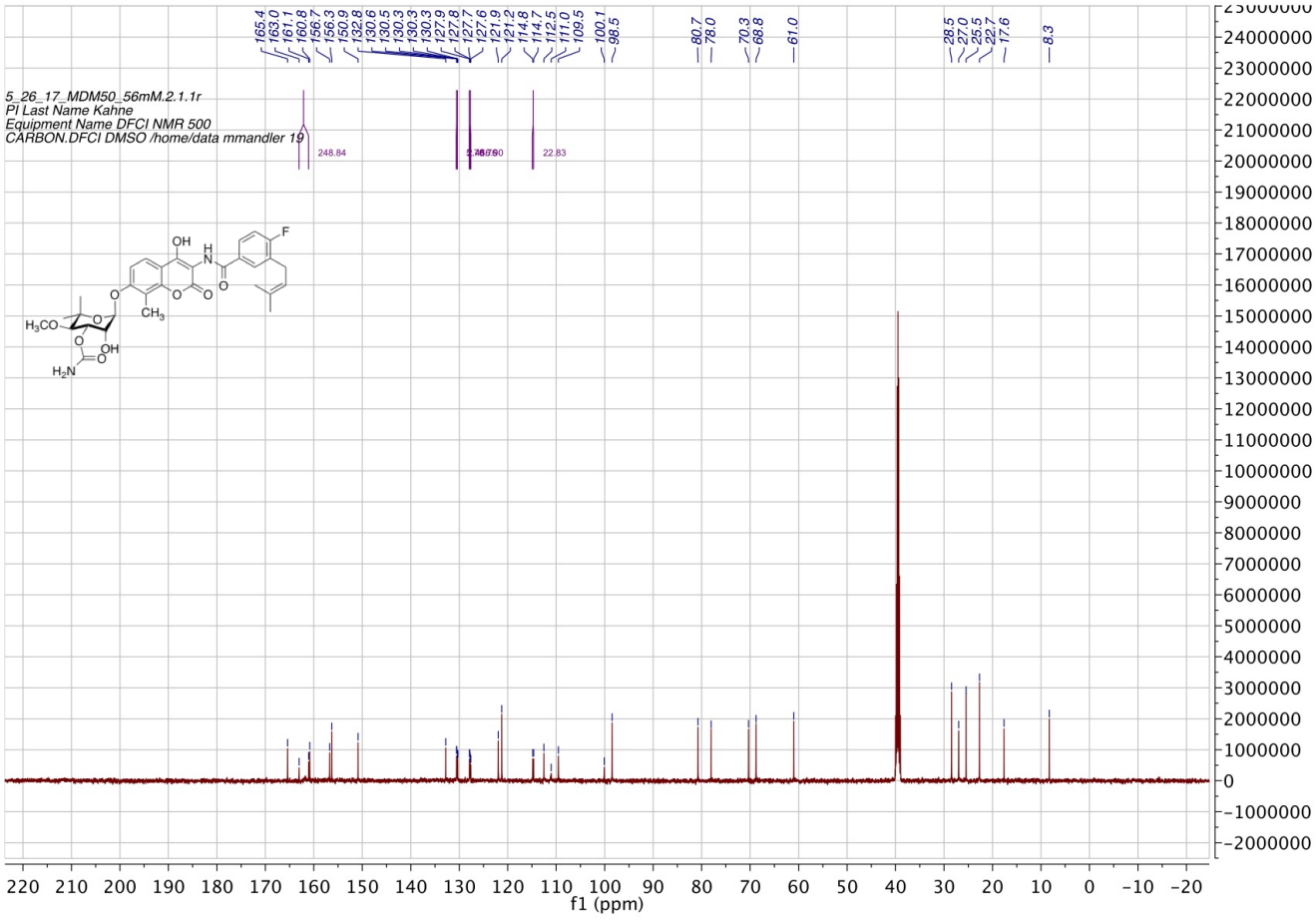

^{19}F NMR of fluorobiocin (fbn)

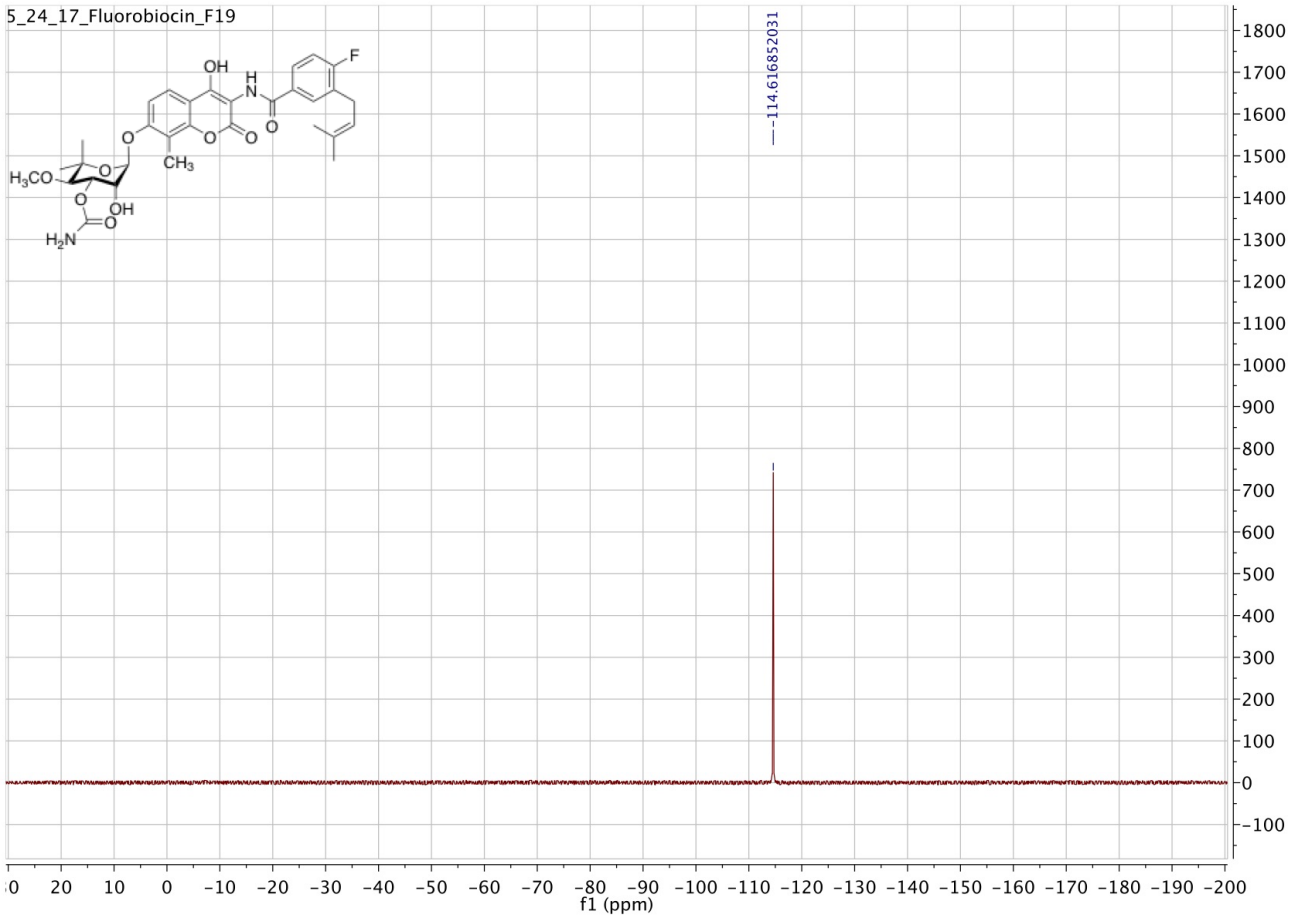

LptB-Fbn NMR Binding Assay

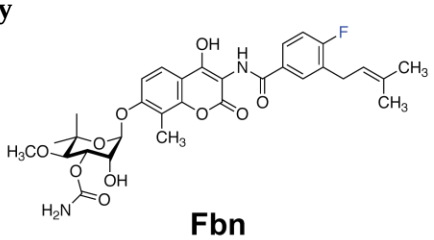

Fbn
Replicate #1

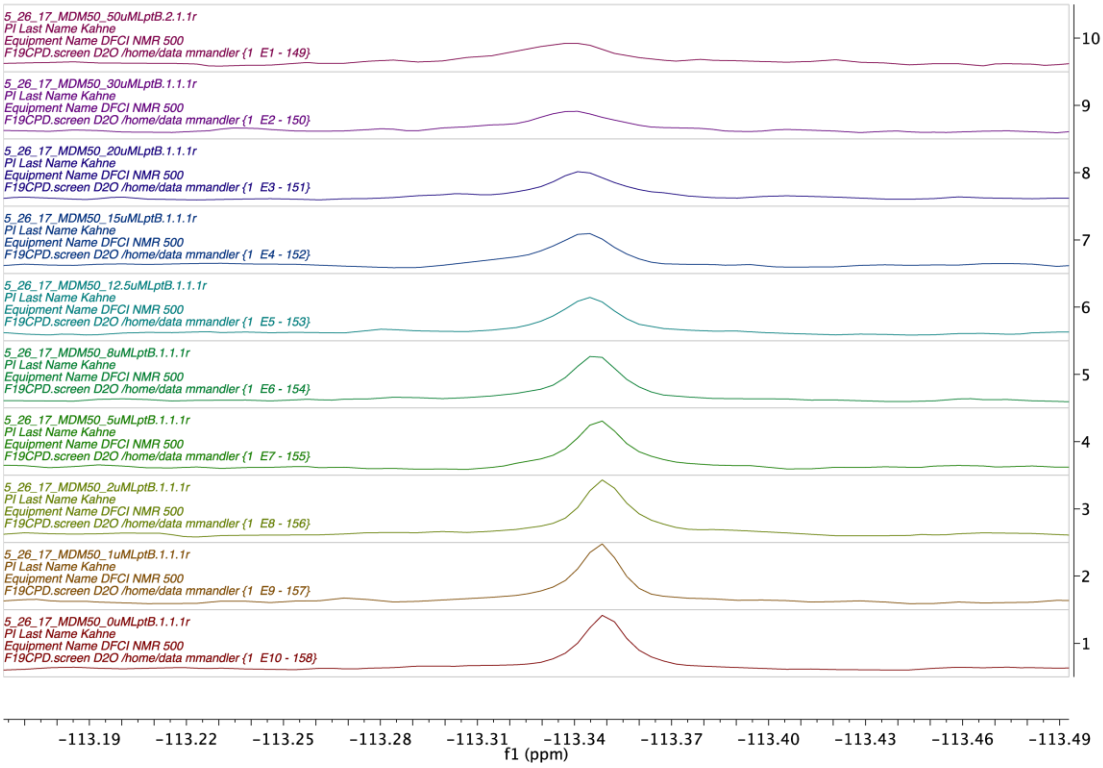

[LptB] (μM)	[Fbn] (μM)
50	50
30	50
20	50
15	50
12.5	50
8	50
5	50
2	50
1	50
0	50

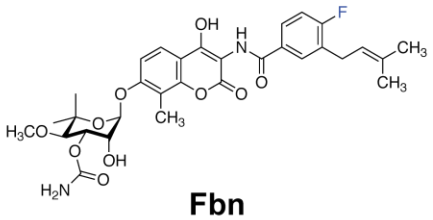

Fbn
Replicate #2

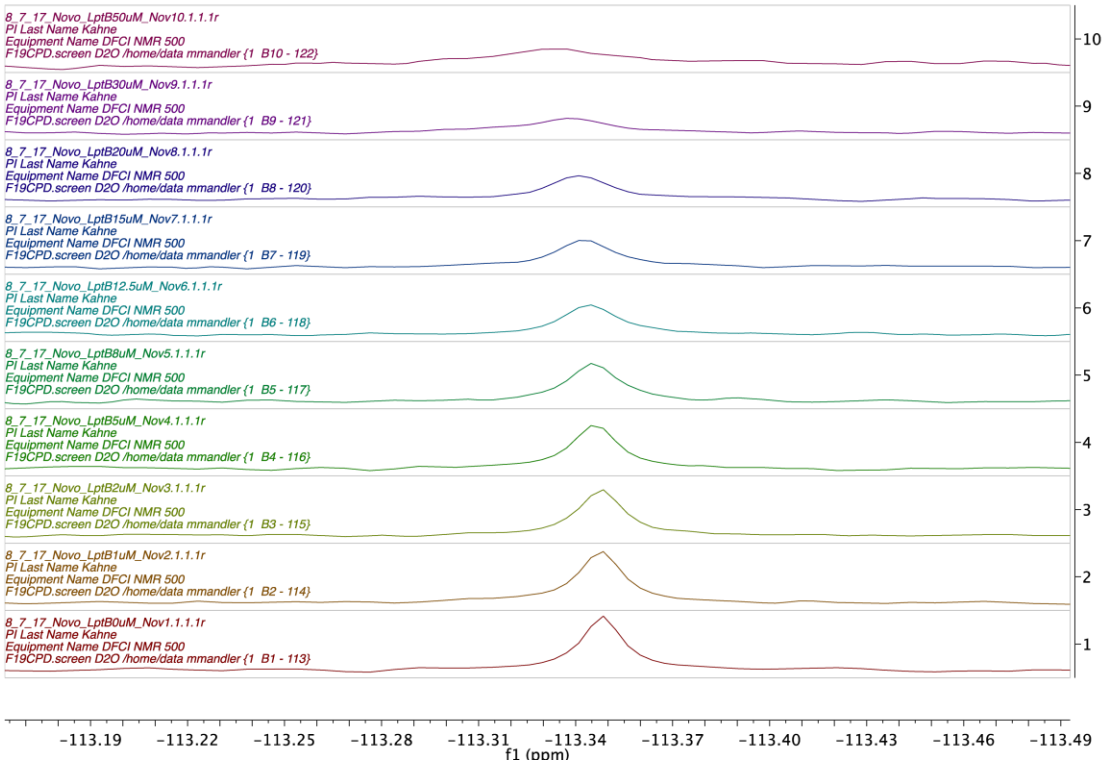

[LptB] (μM)	[Fbn] (μM)
50	50
30	50
20	50
15	50
12.5	50
8	50
5	50
2	50
1	50
0	50

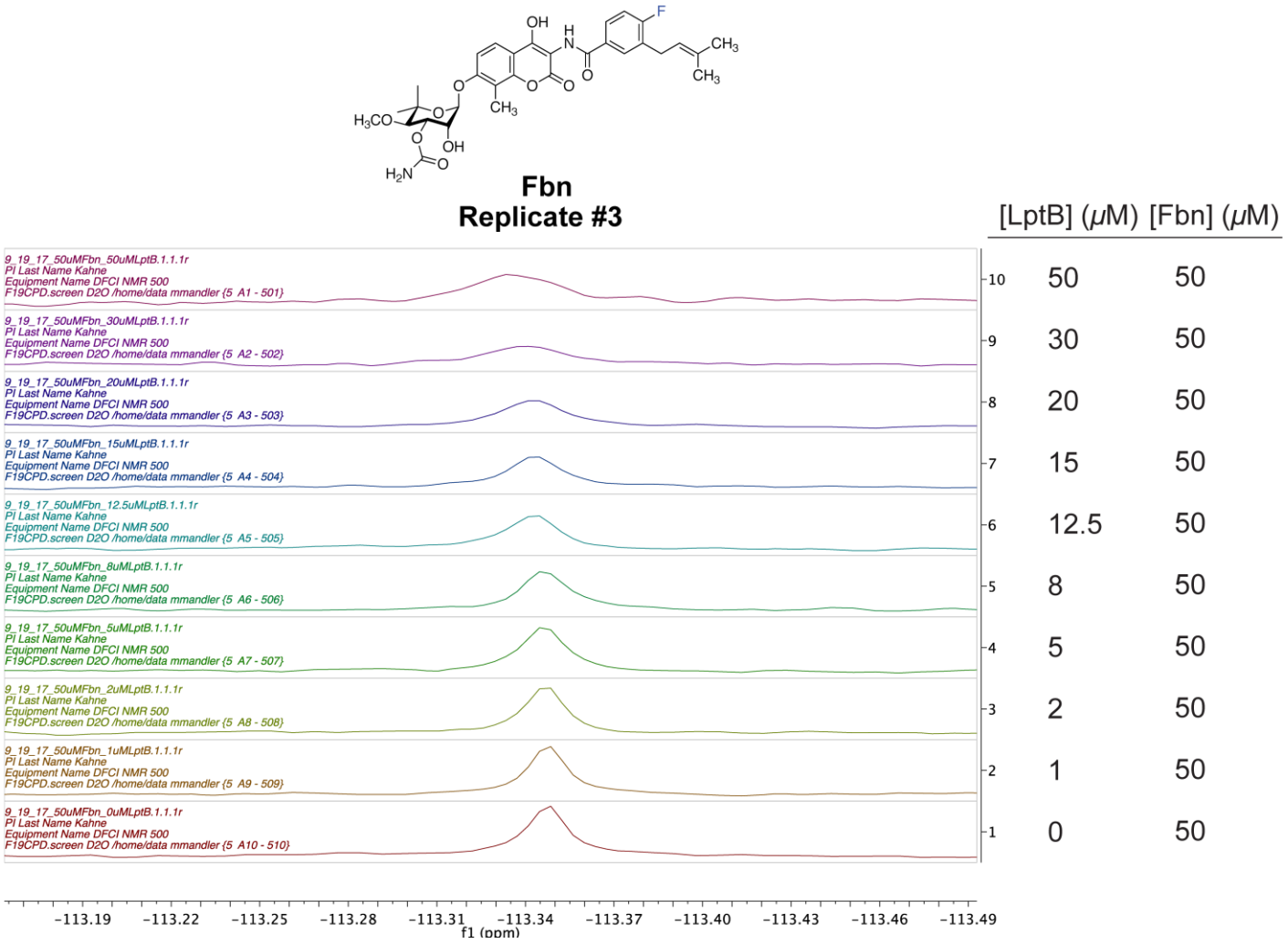

References

1. Yao, Z., Davis, R. M., Kishony, R., Kahne, D., and Ruiz, N. Regulation of bacterial cell size in response to nutrient availability by fatty acid biosynthesis in *Escherichia coli*. *PNAS* **2012,** 109(38), E2561-2568.
2. Luo, Q., Yang, X., Yu, S., Shi, H., Wang, K., Xiao, L., Zhu, G., Sun, C., Li, T., Li, D., Zhang, X., Zhou, M. and Huang, Y. Structural basis for lipopolysaccharide extraction by ABC transporter $LptB_2FG$. *Nat. Struct. Mol. Biol.* **2017**, *24*, 469-474.
3. Davidson, A. L., Dassa, E., Orelle, C. and Chen, J. Structure, function, and evolution of bacterial ATP-binding cassette systems. *Microbiol. Mol. Biol. Rev.* **2008**, *72*, 317-364.
4. Datsenko KA, Wanner BL. One-step inactivation of chromosomal genes in *Escherichia coli* K-12 using PCR products. Proc Natl Acad Sci U S A. 2000;97(12):6640-5. PubMed PMID: 10829079.
5. Yu D, Ellis HM, Lee EC, Jenkins NA, Copeland NG, Court DL. An efficient recombination system for chromosome engineering in *Escherichia coli*. Proc Natl Acad Sci U S A. 2000;97(11):5978-83. PubMed PMID: 10811905
6. Ruiz, N., Gronenberg, L. S., Kahne, D. and Silhavy, T. J. Identification of two inner-membrane proteins required for the transport of lipopolysaccharide to the outer membrane of *Escherichia coli*. *Proc. Natl. Acad. Sci. USA* **2008**, *105*, 5537-5542.
7. Simpson, B. W., Owens, T. W., Orabella, M. J., Davis, R. M., May, J. M., Trauger, S. A., Kahne, D. and Ruiz, N. Identification of residues in the lipopolysaccharide ABC transporter that coordinate ATPase activity with extractor function. *mBio* **2016**, *7*, e01729.

8. Gronenberg, L. S. and Kahne, D. Development of an activity assay for discovery of inhibitors of lipopolysaccharide transport. *J. Am. Chem. Soc.* **2010**, *132*, 2518-2519.
9. Okuda, S., Freinkman, E. and Kahne, D. Cytoplasmic ATP hydrolysis powers transport of lipopolysaccharide across the periplasm in *E. coli*. *Science* **2012**, *338*, 1214-1217.
10. Ryu, Y. and Schultz, P. Efficient incorporation of unnatural amino acids into proteins in *Escherichia coli*. *Nat. Methods* **2006**, *3*, 263-265.
11. Sherman, D. J., Lazarus, M. B., Murphy, L., Liu, C., Walker, S., Ruiz, N. and Kahne, D. Decoupling catalytic activity from biological function of the ATPase that powers lipopolysaccharide transport. *Proc. Natl. Acad. Sci. USA* **2014**, *111*, 4982-4987.
12. Butler, E. K., Davis, R. M., Bari, V., Nicholson, P. A. and Ruiz, N. Structure-function analysis of MurJ reveals a solvent-exposed cavity containing residues essential for peptidoglycan biogenesis in *Escherichia coli*. *J. Bacteriol.* **2013**, *195*, 4639-4649.
13. Leslie, A. and Powell, H. Processing diffraction data with Mosflm. *Evolving Methods for Macromolecular Crystallography* **2007**, *235*, 41-51.
14. Winn, M. D., Ballard, C. C., Cowtan, K. D., Dodson, E. J., Emsley, P., Evans, P. R., Keegan, R. M., Krissinel, E. B., Leslie, A. G. W., McCoy, A., McNicholas, S. J., Murshudov, G. N., Pannu, N. S., Potterton, E. A., Powell, H. R., Read, R. J., Vagin, A. and Wilson, K. S. Overview of the CCP4 suite and current developments. *Acta Crystallogr. D* **2011**, *D67*, 235-242.
15. Evans, P. R. and Murshudov, G. N. How good are my data and what is the resolution? *Acta Crystallogr. D* **2013**, *D69*, 1204-1214.
16. McCoy, A. J., Grosse-Kunstleve, R. W., Adams, P. D., Winn, M. D., Storoni, L. C. and Read, R. J. Phaser crystallographic software. *J. Appl. Crystallogr.* **2007**, *40*, 658-674.
17. Adams, P. D., Afonine, P. V., Bunkoczi, G., Chen, V. B., Davis, I. W., Echols, N., Headd, J. J., Hung, L. W., Kapral, G. J., Grosse-Kunstleve, R. W., McCoy, A. J., Moriarty, N. W., Oeffner, R., Read, R. J., Richardson, D. C., Richardson, J. S., Terwilliger, T. C. and Zwart, P. H. Phenix: a comprehensive Python-based system for macromolecular structure solution. *Acta Crystallogr. D* **2010**, *D66*, 213-221.
18. Chen, V. B., Arendall, W. B., Headd, J. J., Keedy, D. A., Immormino, R. M., Kapral, G. J., Murray, L. W., Richardson, J. S. and Richardson, D. C. MolProbity: all-atom structure validation for macromolecular crystallography. *Acta Crystallogr. D* **2010**, *D66*, 16-21.
19. Afonine, P. V., Grosse-Kunstleve, R. W., Echols, N., Headd, J. J., Moriarty, N. W., Mustyakimov, M., Terwilliger, T. C., Urzhumtsev, A., Zwart, P. H. and Adams, P. D. Towards automated crystallographic structure refinement with phenix.refine. *Acta Crystallogr. D* **2012**, *68*, 352-367.
20. Emsley, P., Lohkamp, B., Scott, W. and Cowtan, K. Features and development of Coot. *Acta Crystallogr. D* **2010**, *66*, 486-501.
21. Painter, J. and Merritt, E. A. Optimal description of a protein structure in terms of multiple groups undergoing TLS motion. *Acta Crystallogr. D* **2006**, *62*, 439-450.
22. Moriarty, N. W., Grosse-Kunstleve, R. W. and Adams, P. D. electronic Ligand Builder and Optimization Workbench (eLBOW): a tool for ligand coordinate and restraint generation. *Acta Crystallogr. D* **2009**, *65*, 1074-1080.
23. Morin, A., Eisenbraun, B., Key, J., Sanschagrin, P. C., Timony, M. A., Ottaviano, M. and Sliz, P. Collaboration gets the most out of software. *eLife* **2013**, *2*, e01456.
24. The Pymol Molecular Graphics System, Version 1.7 Schrodinger, LLC.
25. Chng, S.-S., Gronenberg, L. S. and Kahne, D. Proteins required for lipopolysaccharide assembly in *Escherichia coli* form a transenvelope complex. *Biochemistry* **2010**, *49*, 4565-4567.
26. Villa, R., Martorana, A. M., Okuda, S., Gourlay, L. J., Nardini, M., Sperandeo, P., Deho, G., Bolognesi, M., Kahne, D. and Polissi, A. The *Escherichia coli* Lpt transenvelope protein complex for lipopolysaccharide export is assembled via conserved structurally homologous domains. *J. Bacteriol.* **2013**, *195*, 1100-1108.
27. Gunaherath, G. M. K. B., Marron, M. T., Wijeratne, E. M. K., Whitesell, L. and Gunatilaka, A. A. L. Synthesis and biological evaluation of novobiocin analogues as potential heat shock protein 90 inhibitors. *Bioorg. Med. Chem.* **2013**, *21*, 5118-5129.